coasts

MDPI

Article

Assessing Coastal Flood Risk Under Climate Change with Public Data and Simple Tools: The Geomorphological Coastal Flood Index Applied to the Western Mediterranean

César Mosso [1,*], Manuel Viñes [1,*], Carlos Astudillo [1], Vicente Gracia [1], Daniel González [1], Felícitas Calderón-Vega [2], Joan Pau Sierra [1] and Agustín Sánchez-Arcilla [1]

[1] Laboratori d'Enginyeria Marítima, Department of Civil and Environmental Engineering, Civil Engineering School (Campus Nord), Universitat Politècnica de Catalunya BarcelonaTech, c/Jordi Girona 1-3, 08034 Barcelona, Spain; carlos.astudillo@upc.edu (C.A.); vicente.gracia@upc.edu (V.G.); daniel.gonzalez-marco@upc.edu (D.G.); joan.pau.sierra@upc.edu (J.P.S.); agustin.arcilla@upc.edu (A.S.-A.)

[2] Department of Civil and Environmental Engineering, Universidad de Guanajuato, Juárez 77, Zona Centro, Guanajuato 36000, Mexico; f.calderon@ugto.mx

* Correspondence: cesar.mosso@upc.edu (C.M.); manuel.vines@upc.edu (M.V.)

Abstract

The Mediterranean coast is known for its great tourist attractions, concentration of population, and economic activities. Specifically, in the autonomous regions like Catalonia and Valencia, more than half of the population lives in coastal counties, and the population during the summer months increases due to the influx of tourists. Furthermore, in this stretch of coast, there are some areas of natural interest such as the Delta del Ebro or the Albufera, which are two of the most important wetland areas in the Mediterranean. However, according to studies by Day Today, the retreat of the coastline has increased in recent years, and this influences management of coastal territory both directly and indirectly, mostly harming all sectors with low levels, creating spaces with significant problems. It is for this reason that reporting on climate change and the impact on the coasts is assuming an important role in society, because they are essential tools for planning and management costs. In this thesis, the ground that would be affected by a +1 m, +2 m, and +3 m increase in average sea level, as simulated by the existing flood simulator, has been quantified. And a methodology has been developed for determining the vulnerability of the land based on flooding provided by terrain elevations, and each area studied was evaluated with different degrees of vulnerability: very high, high, moderate, or low. Finally, a first estimate has been made of economic loss that could involve a meter rise in the average sea level for Catalan beaches, and major damage to natural parks, urban areas, and major infrastructure has been identified. This study shows that there are nine areas with high vulnerability due to the low heights of their territory, and the majority of the flooded land is concentrated in the Ebro Delta and the Albufera, which jointly dominate the totals across scenarios.

Keywords: climate change; sea level rise; permanent flooding; flooded land area; geomorphology coastal flooding index

check for updates

Academic Editor: Rafael J. Bergillos

Received: 23 July 2025
Revised: 29 August 2025
Accepted: 20 October 2025
Published: 1 November 2025

Citation: Mosso, C.; Viñes, M.; Astudillo, C.; Gracia, V.; González, D.; Calderón-Vega, F.; Sierra, J.P.; Sánchez-Arcilla, A. Assessing Coastal Flood Risk Under Climate Change with Public Data and Simple Tools: The Geomorphological Coastal Flood Index Applied to the Western Mediterranean. *Coasts* **2025**, *5*, 42. https://doi.org/10.3390/coasts5040042

Copyright: © 2025 by the authors. Licensee MDPI, Basel, Switzerland. This article is an open access article distributed under the terms and conditions of the Creative Commons Attribution (CC BY) license (https://creativecommons.org/licenses/by/4.0/).

1. Introduction

Coastal zones are among the most densely populated and economically vital regions globally, yet they remain acutely vulnerable to the impacts of climate change, particularly sea-level rise (SLR) (e.g., [1,2]). The Spanish Mediterranean coast, especially Catalonia

and the Valencian Community, exemplifies this vulnerability. These regions combine high demographic pressure, intensive tourism, critical infrastructure, and environmentally sensitive systems, such as the Ebro Delta and the Albufera Natural Park, often situated at or near current sea level and exposed to wave overtopping [3–5].

The Intergovernmental Panel on Climate Change (IPCC) projects that global mean sea levels may rise by 0.26–0.82 m by 2081–2100 relative to 1986–2005 under different Representative Concentration Pathways (RCP) scenarios [6]. These projections refer to global mean sea-level changes and should not be interpreted as local forecasts for this study. Local relative sea-level rise (RSLR) depends on regional ocean dynamics and vertical land motion; where site-specific planning requires it, observational datasets (e.g., tide gauges, satellite altimetry, and geodetic estimates of vertical land motion) can be incorporated in follow-on, locally tailored assessments to refine exposure estimates. However, when compounded by regional factors, such as wave climate, storm surges, and wave-induced set-up, SLR in low-lying coastal lacustrine areas or deltaic systems may exceed these bounds.

The Mediterranean is recognized as a coastal hotspot due to its semi-enclosed geometry, limited tidal range, and accelerated relative SLR, which may exceed global averages by ~25% [7]. In response, [8] proposed coastal adaptation pathways tailored to Mediterranean conditions, combining engineering and nature-based solutions to prevent irreversible tipping points.

Low-lying coastal areas, especially deltaic systems, are disproportionately threatened by SLR not only due to their elevation but also because of ongoing land subsidence. This subsidence, driven by both natural processes (e.g., sediment compaction, tectonics) and anthropogenic activities (e.g., groundwater extraction, infrastructure loading), can amplify relative SLR by up to two orders of magnitude compared to global averages [9]. As a result, deltas such as the Ebro are experiencing effective SLR rates far exceeding eustatic trends, increasing their exposure to permanent inundation, aquifer salinization, and infrastructure degradation [10]. Moreover, comparative analyses of global deltas show that vulnerability, measured in terms of flooded land area and population at risk, is strongly correlated with subsidence, storm surge height, and delta area, rather than with SLR alone [11].

Recent research by [12] further emphasizes the growing risk of permanent inundation in Mediterranean urban coastal zones. Their study introduces a high-resolution operational hydrodynamic forecasting system for beaches in Barcelona, demonstrating that the combined effects of storm events and rising mean sea levels can lead to severe impacts, even during short-duration episodes, highlighting the importance of predictive tools and frequent updates to topobathymetric data to maintain flood forecasting accuracy [13]. These findings reinforce the notion that SLR not only increases the frequency of extreme events but also contributes to a growing risk of chronic and irreversible coastal flooding.

Studies on the Valencian coast have shown that urbanized beach segments lacking dunes or natural barriers display significantly higher vulnerability, especially when assessed using integrated Coastal Vulnerability Indices (CVIs) that account for geomorphology, wave exposure, and anthropogenic pressures. Reference [1] applied a hybrid pseudo-dynamic flood modeling approach along the Catalan coast, combining static inundation with habitat conversion analysis. Their findings underscore the pivotal role of local topography and land use in determining exposure and resilience, with natural systems occasionally acting as effective buffers.

Despite growing media attention, spatially explicit, regionally focused analyses along the Mediterranean coast between l'Estartit (Girona) and Cullera (Valencia) remain scarce. Previous work using digital elevation models (DEMs) and static bathymetric flood modeling under SLR scenarios (+1 m, +2 m, +3 m) has simulated potential territorial impacts, but often lacks integrated vulnerability assessment.

This study examines a ~480 km of Mediterranean coastline from l'Estartit to Cullera (Figure 1), covering both Catalonia and Valencia. The region features diverse coastal landforms like deltas, wetlands, urbanized beaches, industrial ports, and natural parks, and is characterized by high socio-economic intensity and ecological sensitivity, making it a representative testbed for Mediterranean coastal vulnerability.

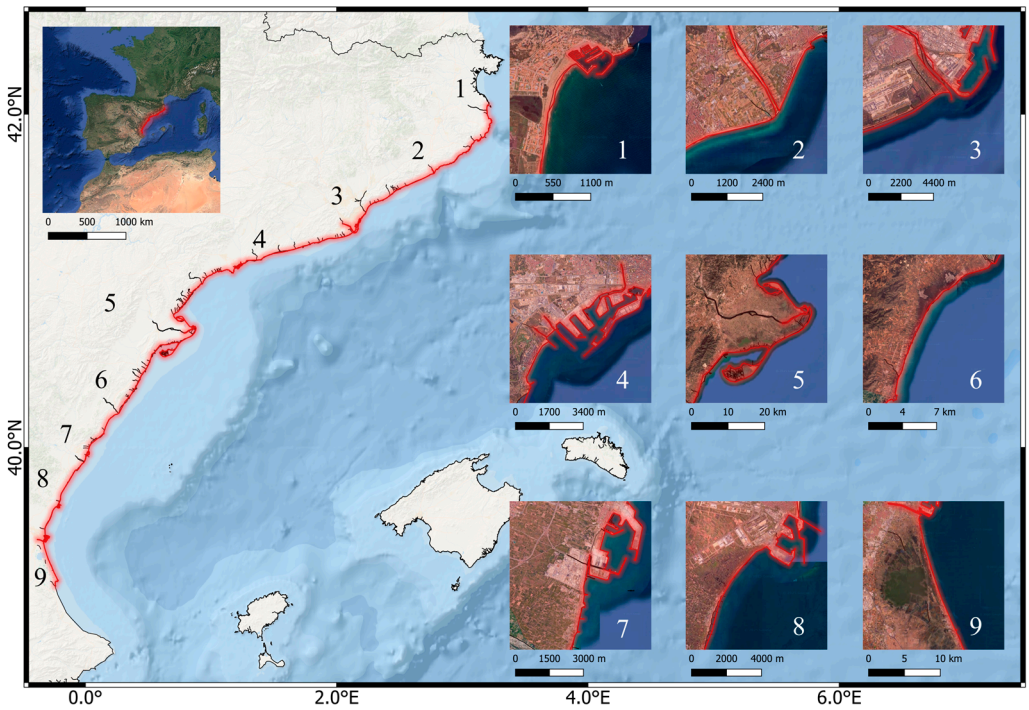


Figure 1. Geographical distribution of key coastal zones analyzed in this study, from L'Estartit (1) in the north to the Albufera Natural Park (9) in the south. Insets show satellite views of each area with the shoreline under the sea-level-rise scenarios considered; numbers correspond to site IDs used throughout. Insets depict static, elevation-based inundation under elevated mean sea level and do not account for existing coastal defenses or their performance; they are intended as upper-bound "no-defense/defense-failure" screening visuals for contingency planning and risk communication.

To address this, the study proposes a three-tiered methodology that is transparent, replicable, and suitable for data-scarce scenarios by:

- Quantifying coastal inundation areas under +1, +2, and +3 m SLR using static bathtub-style flood maps derived from Google Earth's Firetree;
- Evaluating the sensitivity of inundation estimates by testing image resolution and pixel-alignment effects;
- Applying a geometric Geomorphological Coastal Flooding Index (GCFI) based on normalized width, length, and flooded area indicators, developed to classify inundated zones by shape, inland penetration, and surface impact.

This integrative approach identifies critical exposure hotspots and provides preliminary estimates of economic loss, particularly through beach area contraction and its implications for tourism revenue, and is designed for general applicability in coastal planning contexts. This approach aligns with the recent study by [14], which successfully applied a similar protocol to Amazonian barrier beaches, using multi-indicator vulnerability indices for shoreline erosion assessment. This work builds upon that paradigm by explicitly integrating image-based uncertainty analysis and geometric vulnerability metrics, thereby reinforcing the robustness and transparency of coastal SLR impact assessments. A topography-only, static inundation screening approach is applied throughout this study. Dynamic processes such as wave run-up and set-up, storm surge, tidal or compound

events, surface roughness, and the partial performance of coastal defenses are excluded and are discussed as limitations in Section 4. Shoreline erosion and retreat are not modeled, as these require morphodynamic processes that fall outside the scope of this static, topography-based assessment.

The remainder of the article is structured as follows. Section 2 outlines the datasets, image-processing workflows, and analytical procedures for calculating the permanently flooded area and the GCFI. Section 3 presents results: SLR-based inundation quantification (Section 3.1), followed by resolution sensitivity (Section 3.2), uncertainty estimation (Section 3.3), and the GCFI vulnerability indexing (Section 3.4). Section 3.5 offers a comparative review of vulnerability across sites. Finally, Sections 4 and 5 discuss findings and conclusions.

2. Materials and Methods

2.1. Inundation Mapping and Image Acquisition

Flood simulation images were obtained from the public web-based tool flood.firetree.net, which uses elevation data from the National Aeronautics and Space Administration's Shuttle Radar Topography Mission (NASA's SRTM; Washington, D.C., USA.). This tool allows visualization of coastal inundation resulting from SLR scenarios, in 1 m increments from 0 to 60 m above mean sea level. For this study, images were captured for +1 m, +2 m, and +3 m SLR scenarios, using 0 m as the baseline reference. A uniform, SRTM-derived 1 m SLR source was selected to ensure domain-wide consistency and replicability with publicly available inputs across all sites. Incorporating local high-resolution DTMs would compromise comparability and require dataset harmonization, which falls outside the scope of this screening study. The +1 m level is a widely used benchmark for first-order screening in the Mediterranean and can be interpreted as a relative SLR envelope that may combine a gradual rise with local subsidence and/or episodic extremes. The +2 m and +3 m levels are included as stress-test scenarios to explore non-linear sensitivities and bracket uncertainty beyond end-of-century projections. Although the same workflow can be applied to alternative increments or locally projected RSLR values, the standardized 1 m steps ensure internal consistency and reproducibility across sites. As the inputs are static, elevation-based inundation visualizations, the resulting footprints represent no-defense (or defense-failure) conditions and are used for upper-bound screening rather than defended-state forecasting. The elevation data used in this analysis may contain vertical inaccuracies, particularly in low-lying coastal areas with vegetation or urban development, which can affect the precision of absolute flood extent estimates. As this is a screening-level assessment, no ground-truth surveys or site-specific DEM adjustments were conducted; therefore, the results should be interpreted with this limitation in mind.

Images were downloaded in bitmap (BMP) format, ensuring lossless compression, and cropped to a standardized extent of 1349 × 566 pixels [px] across all study areas to maintain spatial comparability. The workflow is viewer-agnostic and can be reproduced from any equivalent SRTM-based (or local DEM-based) set of 1 m SLR inundation rasters providing the same scenarios. Because the workflow operates in image coordinates, all metrics are derived from consistently aligned panels using meters-per-pixel calibration rather than absolute GIS georeferencing, which is not required for the within-site comparisons presented here. We analyzed four scale-bar calibrations at 200 m, 500 m, 1 km, and 2 km, converting pixels to ground distance (m/px) from the on-screen scale bar (Table 1). The 200 m scale was used only in a local sensitivity test as a high-resolution reference, whereas the full study area was processed at 500 m and 2 km to reduce the number of required images while preserving cross-site comparability. Table 1 lists the corresponding pixel-to-

area factors used throughout, and the same calibration was used to generate the scale bars displayed in all figure panels.

Table 1. Scale-bar calibration and derived ground resolution for each level. The scale-bar length in pixels is converted to meters per pixel (m/px) and pixels per km^2, used for pixel-to-area conversion in all analyses.

Measurement Map	Scale [cm Map/cm Real]	Scale	Scale-Bar Calibration [km/px]	Pixels [1 km^2]
200 m	1.3 cm = 200 cm	1:15,384.62	200 m = 49.25 px	60,639.06
500 m	1.7 cm = 500 cm	1:29,411.76	500 m = 62 px	15,376
1 km	1.7 cm = 1 km	1:58,823.53	1 km = 62 px	3844
2 km	1.7 cm = 2 km	1:117,647.06	2 km = 62 px	961

2.2. Image Processing and Flooded Area Calculation

The method involves automated image differencing and thresholding to isolate newly inundated areas at each SLR increment. The steps were as follows:

Preprocessing: Each BMP image downloaded from the simulator includes a wide map area, often containing zones not relevant to the specific coastal site under study. To address this, each image was cropped to extract only the area of interest. This was performed using matrix slicing, which selects a specific portion of the image matrix based on pixel coordinates. This step ensures that all images corresponding to a given site (0 m, +1 m, +2 m, +3 m scenarios) have the same spatial extent and alignment, enabling accurate pixel-by-pixel comparisons. After cropping, all images were converted to grayscale using MATLAB R2021b's rgb2gray function. This transformation simplifies the image to a single intensity channel ranging from 0 (black) to 255 (white), which is sufficient to distinguish flooded (dark blue) zones from land. The resulting grayscale image serves as the basis for binarization and flood detection.

Binary classification: Inundated areas are represented by dark blue tones in the original images. Grayscale pixel thresholds were empirically determined (typically <50 on a 0–255 scale) to binarize each image into flooded (value = 1) and non-flooded (value = 0) zones. This classification was applied to each sea level scenario (0 m, +1 m, +2 m, +3 m).

Differencing: Binary images for each scenario were subtracted pairwise to calculate new inundation extent per meter of SLR (e.g., $A = \text{Flood}_{1m} - \text{Flood}_{0m}$, where matrix A highlights all pixels newly inundated at +1 m SLR). This was repeated for +2 m and +3 m scenarios. Only positive values were retained.

Pixel counting and area conversion: For each difference matrix, the number of flooded pixels was computed. This count was then converted to square kilometers using the specific pixel-to-area ratio derived for each resolution (based on known scale distances). For example, if the scale bar indicates that 62 pixels correspond to 500 m in plain view, then one pixel spans ~8.06 m on the ground. Assuming square pixels, the area per pixel is ~65 m^2. This analysis avoids dependence on external GIS layers; coordinate shifts are immaterial for the reported image-based flooded areas and GCFI calculations given the standardized alignment across scenarios and resolutions.

2.3. Sensitivity Analysis and Error Estimation

A dedicated sensitivity analysis was conducted to assess the impact of image resolution on flooded area estimates. Each zone was analyzed at three spatial scales (low, medium, and high resolution), and the flooded area was calculated as described above. The results were then compared across resolutions for each sea level increment, enabling: (i) Quantification

of the variation in estimated flooded area due to image scale; (ii) Evaluation of stability and robustness of the pixel-count method under different spatial granularities.

In addition, a tolerance-based error analysis was implemented. Given that the exact pixel classification (flooded vs. non-flooded) may be sensitive to boundary conditions or visual artifacts, a $\pm$5-pixel buffer was applied to the flood boundaries to evaluate the upper and lower bounds of inundated area. This approach mimics the uncertainty introduced by manual cropping, low-resolution raster artifacts, or ambiguous terrain elevations near 0 m.

The absolute and relative differences in flooded areas under these variations were recorded and are presented in the Results Section, along with an estimation of uncertainty per site and per inundation scenario. These perturbations are also used to derive lower/upper class assignments for l, w, and a, enabling the computation of [GCFI$^-$; GCFI$^+$] as described in Section 2.4.

2.4. Geomorphological Coastal Flooding Index: Rationale, Development and Design

To translate geometric inundation patterns into a comparative indicator of coastal risk, a Geomorphological GCFI was developed. This index integrates three components (i) the relative alongshore coverage of the inundated strip (percentage of coastline affected) (l); (ii) the relative mean inland reach (mean transect length normal to the coast, expressed as a percentage) (w); (iii) the flooded land area by SLR (a) normalized by the corresponding municipality area. The inundated strip is defined as the sea-connected flood polygon adjacent to the shoreline for each SLR scenario, extracted from the cumulative flooded mask within the analysis frame. A set of transects normal to the coast is used to estimate the mean width and the inland reach contained within the flooded mask. Connectivity to the open sea is enforced to avoid isolated interior depressions below sea level.

Component classes are assigned values from 1 to 4 based on fixed thresholds: for l and w, 1 = <25%, 2 = 25–49%, 3 = 50–74%, and 4 = >75%; for a, 1 = <5%, 2 = 5–10%, 3 = 10–20%, and 4 = >20%. The GCFI (Equation (1)) is grouped into four vulnerability classes: Low (1.0–1.5), Moderate (1.5–2.0), High (2.0–3.0), and Very High (3.0–4.0).

$$\mathrm{GCFI} = \frac{l + w + a}{3} \tag{1}$$

This simplified yet quantitative index enables the integration of spatial descriptors into a synthetic vulnerability score. The use of relative indicators ensures comparability across regions with different absolute sizes, highlighting the influence of geometric configuration rather than only the magnitude of flooding and facilitating spatial comparison among zones, relying solely on planform attributes extracted from freely available elevation-based flood visualizations and highlighting those requiring urgent attention of mitigation planning. This GCFI approach aligns with existing vulnerability frameworks that use geometric or spatial descriptors to assess coastal exposure (e.g., [15,16]). Unlike multi-parameter indices that integrate geomorphological, hydrodynamic, and socioeconomic variables, this formulation focuses exclusively on the physical shape and size of the floodplain, offering a simple yet informative indicator that can be consistently applied across diverse coastal settings. The GCFI is designed for screening with public, image-based inputs, emphasizing the geometry of permanent inundation (alongshore coverage and inland penetration) together with a normalized area term. The workflow relies on static, elevation-based "bathtub" surfaces as inputs; its contribution lies in distilling these surfaces into geometric descriptors, enforcing sea connectivity, and reporting component- and index-level bounds [GCFI$^-$,GCFI$^+$] derived from resolution/tolerance tests. In contrast to multi-parameter coastal vulnerability indices that integrate dynamic forcings, morphodynamics, and sometimes socioeconomic layers, this formulation provides a replicable, data-light

baseline that can be applied consistently across sites and, where data permit, complemented or benchmarked against more data-intensive approaches.

2.5. Uncertainty Quantification

Given that l, w, and a are ordinal classes derived from continuous spatial measurements, bounds for the GCFI are reported by propagating image-based uncertainty. Flood footprints are first perturbed using a ±5-pixel boundary tolerance to simulate edge and classification ambiguity, and the underlying continuous quantities informing l, w, and a are recomputed accordingly. Resolution sensitivity is then addressed through the multi-scale analysis described in Section 2.3. Each perturbation yields lower- and upper-class assignments (l^-, w^-, a^-) and (l^+, w^+, a^+), from which the index bounds are calculated as shown in Equation (2):

$$\mathrm{GCFI}^- = \frac{l^- + w^- + a^-}{3};\ \mathrm{GCFI}^+ = \frac{l^+ + w^+ + a^+}{3} \quad (2)$$

The interval [GCFI^-, GCFI^+] is reported, along with an indication of whether the resulting vulnerability class changes, thereby making class stability explicit.

In this context, the study introduces a novel, pixel-based framework for static flood mapping that enhances traditional "bathtub" methodologies by integrating resolution sensitivity and a GCFI alongside the conventional CVI by combining static flood mapping, uncertainty analysis, and geometric vulnerability indicators into a single, replicable workflow. Unlike standard geographic information systems models, which often depend heavily on detailed DEMs and dynamic modeling tools, our approach leverages publicly available satellite imagery and simple pixel-subtraction routines to deliver high-resolution inundation analysis with minimal computational demand, operable on a standard personal computer. While improved "bathtub" methods require complex data and heavy processing, our pipeline maintains simplicity and scalability, offering a robust first-order exposure assessment even in data- and resource-scarce regions. The GCFI, therefore, does not predict shoreline retreat; it summarizes the geometry of permanent inundation footprints for screening purposes, to be complemented by morphodynamic/erosion assessments in subsequent analyses.

2.6. Study Sites

Nine coastal sites along the Spanish Mediterranean coast were selected for analysis based on their topographic vulnerability, morphological characteristics, and socio-environmental relevance (Figure 1). The selection aimed to represent a variety of geomorphological settings that are particularly sensitive to SLR, including deltas (and their adjacent areas, where the terrain is very flat and sediment supply is limited), coastal lagoons, and low-lying urbanized zones. These latter areas make up a significant portion of the study region, corresponding to tourist beaches or urban coastal strips with high economic value linked to recreational use and infrastructure. The sites were also chosen due to the availability of clear inundation imagery on the flood.firetree.net platform, as well as their importance for coastal management and conservation planning. Together, this set of study areas offers a representative sample of Mediterranean coastal typologies, encompassing both natural systems and urban landscapes. This is especially relevant for evaluating the performance of low-cost, image-based flood models and their applicability in early-stage coastal planning under climate change scenarios. The selected sites include (from north to south).

L'Estartit: A coastal area known for its low cliffs, rocky coves with coarse sand, and proximity to flatlands and restored wetlands. It forms part of a diverse natural landscape within the Montgrí, Medes Islands and Baix Ter Natural Park.

Tordera Delta (Catalonia): A small but dynamic deltaic area at the northern fringe of the Barcelona province, featuring a narrow beach backed by low-lying agricultural and urban land.

Llobregat Delta (Catalonia): Located immediately southwest of Barcelona, this delta contains important infrastructure (e.g., the airport), nature reserves, and urban expansion zones, all within a few meters of mean sea level.

South Tarragona Coast (Catalonia): Includes suburban and semi-natural areas with varying degrees of artificial protection (seawalls, dunes), allowing assessment of contrasting response types.

Ebro Delta (Catalonia): One of the most prominent and vulnerable deltas in the western Mediterranean, with large expanses of land at or below current sea level. It is subject to sediment deficit, subsidence, and high exposure to SLR-induced permanent inundation.

Prat de Cabanes-Torreblanca (Valencia): A natural park with shallow wetlands and marshes, acting as a buffer zone for marine ingress but extremely sensitive to even minor sea level increases due to its flat topography.

Castellón de la Plana (Valencia): An urbanized section of the Valencian coast with artificialized beaches, where both the built environment and infrastructure are potentially at risk from permanent flooding.

Sagunto Coastline (Valencia): Combines residential, industrial, and natural areas; features low topography and modified shorelines, increasing exposure to marine transgression.

Albufera de Valencia (Valencia): A coastal lagoon and wetland system of high ecological value, protected under the Ramsar Convention and Natura 2000 network. It is surrounded by rice fields and low-lying rural settlements, with very limited natural protection from the sea.

Each site was analyzed independently at three spatial resolutions, and flooded areas were calculated for +1 m, +2 m, and +3 m SLR scenarios. The resulting vulnerability assessments allow for inter-site comparison, sensitivity analysis, and ranking of risk levels across this diverse coastal transect.

2.7. Data and Code Availability

All source images were obtained from flood.firetree.net, a publicly accessible tool that does not require registration or login. The MATLAB R2021b code developed for processing the images, extracting flooded areas, and computing the GCFI is available upon reasonable request from the corresponding author. The analysis can be fully replicated using public tools and the methodological framework provided in this manuscript.

3. Results

This section presents the outcomes derived from the application of the proposed methodology for estimating coastal inundation under progressive SLR scenarios, as well as the assessment of vulnerability levels across the selected coastal zones. The structure of the results follows the logical sequence of the methods, aiming to facilitate interpretation and highlight the robustness and scalability of the approach. Initially, the total flooded areas associated with +1 m, +2 m, and +3 m SLR increments are reported and compared across all case study sites. These estimations are then evaluated through a sensitivity analysis focused on the influence of spatial resolution, examining how image scale affects the calculation of inundated areas. An uncertainty analysis is also included, based on pixel

boundary tolerance, to quantify potential variability in the results due to minor image shifts or classification ambiguities.

Subsequent sections present the computation of the GCFI, which incorporates geometric characteristics of inundation to generate a standardized risk indicator. Finally, a comparative ranking of the sites is provided to synthesize vulnerability levels and support further interpretation of spatial patterns and model performance.

3.1. Flooded Area Estimation Under SLR Scenarios

The main aim of this analysis is to quantify the extent of permanent coastal flooding under the projected SLR scenarios of +1 m, +2 m, and +3 m. The total flooded areas were extracted from the binarized difference in satellite-derived images, as described in the methodology, and converted to surface area (km^2) using calibrated image resolution factors (as detailed in Table 1). To illustrate the methodology applied in this study, a representative case is presented for the Ebro Delta. Figure 2 shows the sequence of flood extent visualizations corresponding to SLR scenarios of 0 m, +1 m, +2 m, and +3 m. (extracted from the Firetree global flood map) and converted to grayscale in order to enable pixel-based processing. The grayscale transformation facilitates the numerical comparison between successive inundation stages. Specifically, image subtraction operations were performed to compute the incremental changes in flood extent between consecutive SLR scenarios, that is: (b–a), (c–b), and (d–c), corresponding, respectively, to the increase in inundation from 0 m to +1 m, +1 m to +2 m, and +2 m to +3 m. This process enabled a direct estimation of the area increment and spatial configuration of newly inundated zones for each SLR threshold.

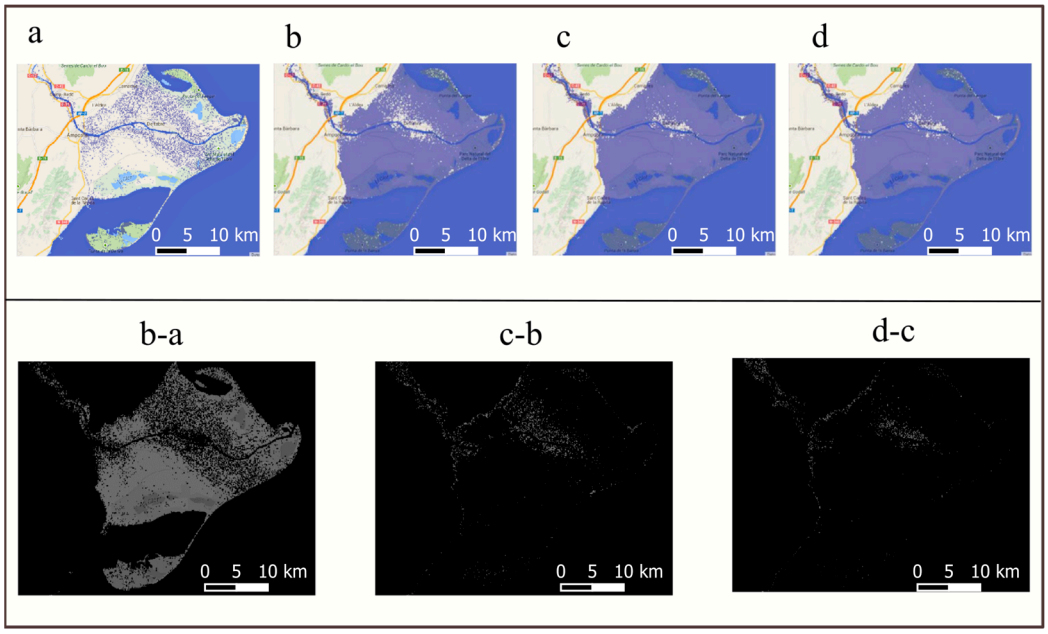


Figure 2. Sequence of flood extent images for the Ebro Delta under increasing SLR scenarios: (**a**) 0 m, (**b**) +1 m, (**c**) +2 m, and (**d**) +3 m. The second row shows the corresponding grayscale versions used for image analysis. The third row displays the differential inundation areas computed by subtracting consecutive scenarios: (b-a), (c-b), and (d-c). This process enabled pixel-based quantification of incremental flooding and supported the estimation of inundated area growth across SLR thresholds. Each sub-panel includes a scale bar to facilitate spatial comparison across scenarios and processing steps. Panels depict static equilibrium inundation under elevated mean sea level and do not account for existing coastal defenses or their performance. As such, they are best interpreted as upper-bound "no-defense/defense-failure" scenarios useful for contingency planning and risk communication.

This approach enabled the identification of spatial patterns of flooding across the diverse geomorphological features of each of the nine study sites. Flood extent (Table 2) of the total area flooded for each site and scenario demonstrates a clear and consistent increase in inundated surface as SLRs, with considerable spatial variability across the selected coastal systems.

Table 2. Total flooded surface area (in km^2) estimated for each study site under three SLR scenarios: +1 m, +2 m, and +3 m. These values were derived from pixel-based analysis of satellite-derived flood maps and represent the cumulative inundated extent per site under each scenario.

Site	SLR	Flooding (km^2)
L'Estartit	+1 m	12.427
	+2 m	22.786
	+3 m	31.805
Tordera Delta	+1 m	0.396
	+2 m	1.378
	+3 m	2.633
Llobregat Delta	+1 m	9.722
	+2 m	21.649
	+3 m	33.891
Tarragona	+1 m	3.052
	+2 m	5.349
	+3 m	7.874
Ebro Delta	+1 m	277.167
	+2 m	295.753
	+3 m	304.544
Prat de Cabanes-Torreblanca	+1 m	10.274
	+2 m	12.19
	+3 m	13.727
Castellón de la Plana	+1 m	21.473
	+2 m	37.018
	+3 m	50.075
Sagunto	+1 m	27.7
	+2 m	45.576
	+3 m	62.136
Albufera de Valencia	+1 m	156.805
	+2 m	183.952
	+3 m	206.301

Among all sites, the Ebro Delta exhibits the most extensive floodplain, with 277.167 km^2 inundated at +1 m SLR, increasing to 295.753 km^2 at +2 m, and reaching 304.544 km^2 at +3 m. This behavior reflects the high exposure of this deltaic environment, characterized by minimal elevation gradients, ongoing subsidence, and extensive wetland and agricultural areas. The Albufera de Valencia ranks second in total inundated area, with flooding expanding from 156.805 km^2 at +1 m to 183.952 km^2 at +2 m and 206.301 km^2 at +3m. This sharp increase underscores the vulnerability of lagoonal systems with low-lying margins and artificially maintained water levels. Similar progressive trends were observed in other Spanish locations such as the Doñana wetlands [17], the Albufera de Valencia [18] and the Mar Menor [19].

Intermediate values are observed in the coastline of Valencia (Sagunto, Castellón de la Plana) and urban deltaic systems in Catalonia (Llobregat Delta and L'Estartit), where flood extent is constrained by topographic variation and anthropogenic modifications.

These results are consistent with existing projections in the scientific literature, which demonstrate that low-lying coastal regions, especially deltas, lagoons, and estuarine plains, are highly susceptible to even modest increases in sea level [20,21]. Studies using DEMs and hydrodynamic models have similarly found that +1 to +3 m SLR can cause extensive permanent inundation in many Mediterranean and subtropical coastlines [22,23]. The pixel-based method employed here offers a simplified but effective means of replicating such projections using readily accessible geospatial imagery, albeit with less vertical precision.

The variation in flooded area among sites also reflects local geomorphology and coastal slope. Regions with flatter topography (such as the Ebro Delta or the Albufera) are more prone to extensive horizontal transgression of floodwaters, whereas steeper coastlines display more limited inundation. This confirms prior research highlighting the influence of topographic slope and elevation gradients on SLR-driven exposure [24,25]. These factors must be carefully considered in coastal planning, as they modulate the spatial distribution of risk and the potential for ecosystem or infrastructure loss.

3.2. Sensitivity to Spatial Resolution

The accuracy of flood extent estimation based on image analysis is highly sensitive to the spatial resolution of the input data. This section examines how different map resolutions influence flood extent estimations (m/px, as detailed in Table 1) by comparing the resolutions used in this study: a finer resolution (500 m) and a coarser resolution (2 km). In the local sensitivity test, an additional 200 m and 1 km scale-bar levels were used to quantify relative error with respect to the 200 m reference (see Section 3.3). Pixel-to-area conversion factors, derived from the values in Table 1, were applied to translate the number of inundated pixels into flooded surface area (km^2) for each SLR scenario. In this context, the methodology enhances the interpretability of static inundation outputs by reporting component-level bounds and GCFI ranges rather than attempting to correct the physical limitations of bathtub inputs.

The results of the total flooded area for each scenario (+1 m, +2 m, +3 m SLR) are summarized in Table 3. Across all cases, there is a consistent overestimation of the flooded area when using the coarser-resolution map. For example:

- Under +1 m SLR, the flooded area was 528.72 km^2 using the 500 m map, compared to 562.08 km^2 with the 2 km map, representing a relative overestimation of 6.3%.
- Under +2 m SLR, the respective values were 713.31 km^2 and 736.32 km^2, corresponding to a difference of 3.2%.
- Under +3 m SLR, the overestimation reached 3.1%, with areas of 846.76 km^2 (500 m) and 873.15 km^2 (2 km).

Table 3. Total results for the study area for two types of maps with a tolerance of 0 and 5 pixels. As well as percentage of flood increase.

Map	Tolerance	Level of Inundation [m]	Pixels [px]	Affected km^2	Percentage Increase in Flooding [%]
500 m	0	+1 m	8,129,618	528.721	21.947
		+2 m	9,913,835	644.760	
		+3 m	11,425,777	743.092	15.251
	5	+1 m	8,127,125	528.559	21.948
		+2 m	9,910,852	644.566	
		+3 m	11,422,532	742.881	15.253

Table 3. *Cont.*

Map	Tolerance	Level of Inundation [m]	Pixels [px]	Affected km^2	Percentage Increase in Flooding [%]
2 km	0	+1 m	540,157	562.078	20.990
		+2 m	653,534	680.056	
		+3 m	749,676	780.100	14.711
	5	+1 m	539,967	561.880	20.992
		+2 m	653,319	679.832	
		+3 m	749,442	779.856	14.713

This outcome is consistent with prior research. Several authors have documented that coarser-resolution DEMs tend to overestimate flood extents because they smooth out microtopographic barriers that would otherwise confine floodwaters in finer-scale models [26,27]. In such cases, the pixel-scale representation allows partial flooding in a cell to be interpreted as full inundation, thus inflating the computed surface area [28]. Furthermore, studies have shown that flood extent and water depth can vary linearly with DEM resolution, emphasizing the importance of choosing an appropriate scale [29].

The influence of resolution appears to be more significant under low SLR scenarios, where flooding affects narrow or discontinuous coastal strips. In these cases, fine-scale spatial detail is essential to accurately capture the extent and shape of inundated zones. As the SLR scenario increases, the flooded areas expand, and differences between resolutions diminish in relative terms, although they remain relevant in absolute terms.

While high-resolution data generally improve flood extent prediction accuracy, they also impose greater computational costs and data storage requirements [30]. For large-scale assessments, the trade-off between spatial detail and efficiency becomes critical. Coarse-resolution datasets may be acceptable for regional risk screening but are inadequate for site-specific vulnerability mapping or infrastructure planning, where small-scale features significantly influence flood pathways and exposure patterns [31].

Moreover, vertical accuracy also plays a key role. Global elevation datasets such as NASA's SRTM, despite their relatively high horizontal resolution (~30 m), have known vertical biases in vegetated or urban areas. These biases can lead to significant underestimation of the population and assets at risk, as demonstrated by [25], who found that SRTM-based assessments omitted up to 60% of the exposed population in some U.S. states when compared to high-accuracy Light Detection And Ranging (LiDAR) based models.

To complement the resolution analysis, a pixel tolerance evaluation was conducted by introducing a buffer of ± 5 pixels to simulate spatial uncertainty had minimal impact on the total flooded area (less than 1% deviation across all SLR levels). This result suggests that the method used is robust to minor positional shifts and confirms that the primary source of sensitivity in this analysis is the spatial resolution rather than the edge tolerance.

In summary, the spatial resolution of flood mapping inputs exerts a measurable and systematic influence on inundation estimates. Coarser data tend to overestimate flooded areas due to generalized representation of terrain and loss of microtopographic control. These biases must be explicitly considered when applying image-based methods to coastal vulnerability studies. For accurate and policy-relevant results, the selection of spatial scale should match the intended use, with high-resolution inputs favored for localized impact assessments and adaptation planning.

3.3. Uncertainty Estimation from Image Tolerance

In addition to spatial resolution, the reliability of flooded area estimates may be affected by image classification thresholds, pixel alignment, and edge detection variability. To evaluate the robustness of the method, a pixel tolerance test was conducted by comparing inundation estimates under two scenarios: a strict classification threshold (0-pixel tolerance) and a relaxed one allowing ±5-pixel margin around flood boundaries. This approach simulates minor shifts in segmentation or classification errors that may arise from image preprocessing or resolution-induced artifacts (see Table 4).

Table 4. Comparative results for the selected test area using different map scales, showing the affected surface area in km^2 for each SLR scenario and the associated percentage error relative to the 200 m scale. Note: The 200 m level is used only in this local sensitivity analysis as the high-resolution reference; the full study area was computed at 500 m and 2 km.

Scale	Inundation Level [m]	Affected km^2	Percentage of Error with Respect to 200 m Map [%]
200 m resolution	1	1.362	-
	2	2.519	-
	3	3.672	-
500 m resolution	1	1.354	0.59
	2	2.487	1.27
	3	3.624	1.31
1 km resolution	1	1.335	1.98
	2	2.431	3.49
	3	3.569	2.81
2 km resolution	1	1.288	5.43
	2	2.373	5.80
	3	3.513	4.33

The results indicate that pixel tolerance had a negligible effect on overall flooded area estimates across all SLR scenarios. Differences between 0-pixel and 5-pixel tolerance configurations were below 1.2% for all cases, confirming the robustness of the method. These findings are in agreement with prior studies that evaluated the sensitivity of raster-based flood mapping to positional uncertainty and segmentation thresholds. For instance, [30] showed that horizontal spatial uncertainty in coarse DEMs had a limited impact on total inundation extent in large-scale coastal regions, although effects could be locally significant. Similarly, [32] found that uncertainty due to vertical and horizontal positioning is often overshadowed by other factors such as elevation error or hydrodynamic variability.

3.4. Performance Assesment of the Geomorphological Coastal Flooding Index

To synthesize the results of the flooding scenarios into a unified vulnerability metric, the proposed GCFI is computed according to Equation (1), which relates the flooded area, the geometrical complexity of the flood footprint, and the SLR through a normalized ratio.

This formulation is consistent with approaches that prioritize simplicity, transparency, and replicability in spatial vulnerability assessments (e.g., [16,33]). By integrating both the extent and configuration of the flooded surface, this index captures both the magnitude of potential impacts and their spatial morphology, which is an important factor for risk perception and for the design of adaptive management policies. All variables were normalized to allow comparison across case studies, regardless of their absolute size. The resulting GCFI values, computed for each SLR scenario (+1 m, +2 m, and +3 m), are summarized comparatively in Figure 3.

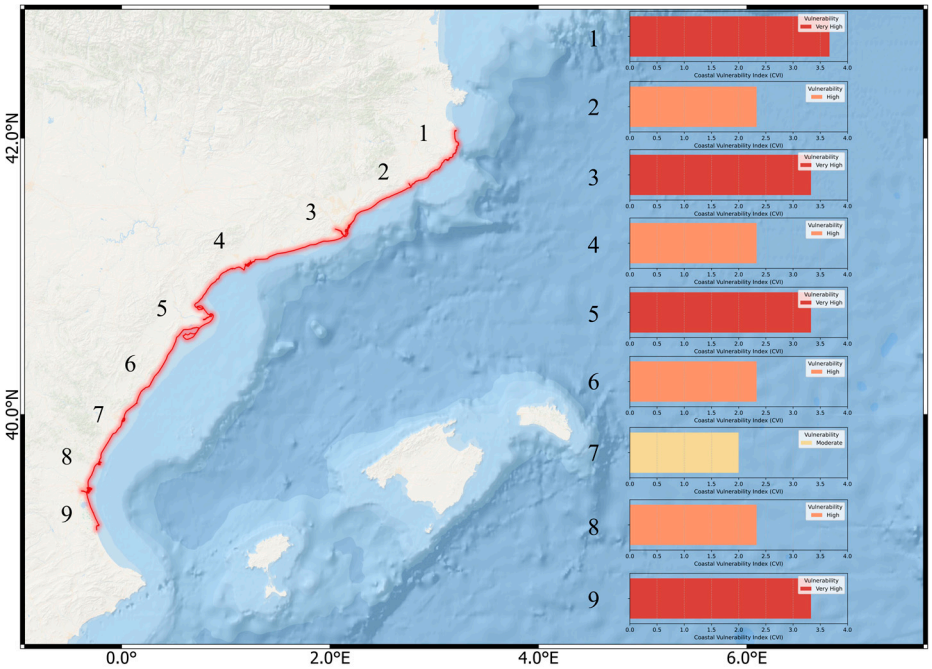


Figure 3. Geographical distribution of the GCFI along the Catalan and Valencian Mediterranean coast. The map displays GCFI values calculated for each of the nine study sites under the considered SLR scenarios (+1 m, +2 m, and +3 m) categorized into three vulnerability classes: Moderate, High, and Very High. The index integrates the extent and spatial configuration of flood footprints, normalized to enable comparison across sites of varying sizes. This visualization supports a comparative assessment of coastal vulnerability, emphasizing both the magnitude and morphology of potential impacts and their physical susceptibility to SLR impacts.

According to the GCFI results, the Ebro Delta consistently exhibits the highest vulnerability, reflecting its expansive and elongated inundation pattern under all SLR scenarios. The Albufera de Valencia also shows very high values. The intermediate to low GCFI corresponds to a more compact and spatially confined flood geometry, which is in line with previous coastal sensitivity studies highlighting the role of topographic setting, floodplain openness, and inland penetration in shaping flood exposure (e.g., [34,35]), indicating either greater perimeter length for a given area or a more fragmented and irregular flood zone, conditions typically associated with higher management complexity and exposure.

3.5. Comparative Ranking of Study Sites

This section presents a comparative summary of the results, focusing on both the GCFI and the flooded area under different SLR scenarios. These indicators are compared for the different study areas, highlighting the importance of the first meter of SLR, which in many cases has the greatest relative impact on the coast. Next, the behavior of the GCFI and the evolution of the flooded area are analyzed separately, emphasizing linear or non-linear flooding patterns with SLR, and regional differences (e.g., Ebro Delta vs. other areas) are discussed. Finally, the implications in terms of beach loss and tourism and the vulnerability of study are addressed.

3.5.1. Link Between SLR and Flooded Area

The mapping of flood-prone areas under +1 m, +2 m, and +3 m SLR reveals site-dependent behaviors (Figure 4). For clarity, Figure 4 is presented in two panels: (a) a full-scale view including the Ebro Delta and the Albufera, and (b) the same data with a truncated y-range to improve readability for the remaining sites; both panels use the same y-axis units (km^2) and no secondary y-axis is employed. Across the study domain, the increase

in flooded area reflects the prevailing geomorphology. In several sites (e.g., L'Estartit, Llobregat Delta), successive 1 m increments produce approximately linear responses across the full 0 to +3 m sea level rise range, with similar added flooded areas per meter of SLR. This pattern indicates a progressive, sustained expansion of flooded land without an abrupt regional-scale threshold within the evaluated range. For low-lying deltas and lagoons (e.g., the Ebro Delta), these static extents should be interpreted as upper-bound exposure; defended-state projections would require site-specific, process-based modeling that accounts for defense performance and dynamic forcings. In urbanized settings with existing measures (e.g., dikes and pumping in the Llobregat Delta), defended exposure can be lower than these envelopes; the present curves are therefore interpreted as upper-bound, no-defense/defense-failure screening.

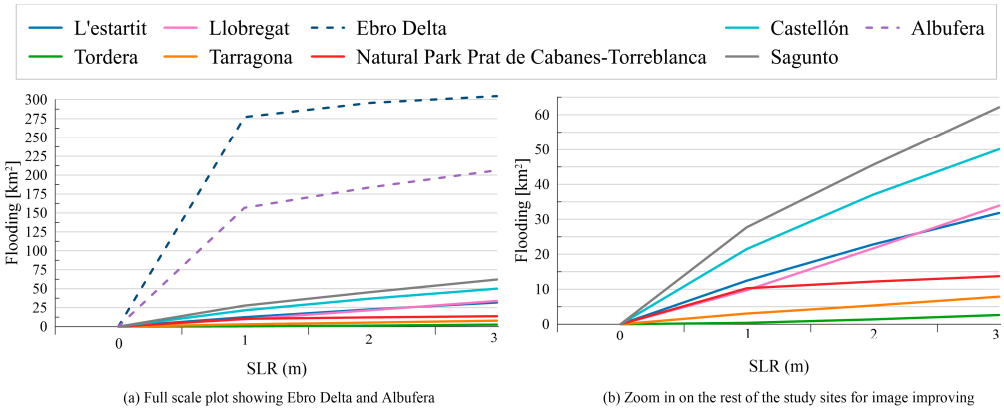


Figure 4. Relationship between flooded area and SLR across the nine study sites along the Catalan and Valencian coast. Panel (**a**) shows the full-scale evolution of flood-prone areas, highlighting the dominance of the Ebro Delta and the Albufera. Panel (**b**) presents a zoom on the remaining sites to improve visibility of smaller-scale responses. The plot illustrates how the extent of flood-prone areas evolves under three SLR scenarios (+1 m, +2 m, and +3 m). While some locations (e.g., L'Estartit, Llobregat Delta) exhibit a near-linear increase in flooded areas, others (e.g., Tordera Delta, Ebro Delta, Cabanes, Albufera) show non-linear responses, with either concave (decelerating) or convex (accelerating) trends. These patterns reflect the influence of local geomorphological characteristics on flood dynamics.

However, when disaggregated by region or specific units, important non-linear patterns emerge (Tordera Delta, Ebro Delta, Cabanes, and Albufera). In some cases, the curve of flooded area vs. SLR is concave (decelerated), where the first meter floods more than the subsequent ones, until reaching a ceiling. Other curves show a slightly convex (accelerated) shape, indicating that additional SLR will flood proportionally more territory than the first meter. A simple hypsometric proxy corroborates these patterns: in the Ebro Delta, ≈70% of the surface lies below +1 m, consistent with concave responses dominated by the first meter; conversely, the Tordera Delta exhibits a convex pattern (≈15% at +1 m, ≈52% at +2 m, >95% at +3 m), indicating threshold-controlled inland penetration.

This result shows that many low-lying coastal areas do indeed experience most of their increase in flooded areas with the first meter of SLR. This is the case for extensive deltas and marshes: for example, in the Ebro Delta, approximately 70% of its surface area is below +1 m above current sea level [36], which means that a SLR of one meter would put up to ~70% of the delta under water (assuming no protective measures are in place). This is reflected in Figure 4, where the quantification for the Ebro shows that the first meter of elevation causes the flooding of most of the deltaic surface, while the subsequent SLR floods additional smaller areas. In other words, the flooded area vs. SLR curve for the Ebro Delta is concave, saturating quickly. Much of the territory is already affected at +1 m,

and from ~+2 m onwards, the delta would be almost completely flooded (≥85–90% of its area). This result is consistent with previous assessments that characterize the Ebro Delta as an environment that is extremely vulnerable to small changes in sea level due to its topography. Reference [36] estimated that in a scenario of +88 cm by 2100 (AR4 high scenario), up to 61% of the delta could be affected. In fact, detailed calculations indicate that ~50% of the Ebro Delta is below +0.5 m and ~70% below +1 m, which explains the enormous sensitivity to the first meter of SLR. Figure 4 clearly shows this concentration of inundation in the first decimeters/meter of elevation. Another notable case is that of the Albufera de Valencia, which includes a shallow coastal lagoon (average depth ~+1 m) surrounded by ~223 km^2 of very low-lying rice fields, separated from the open sea by a narrow sandy dune cordon. The results show that the first meter of SLR would be the most damaging in the Albufera basin. Thus, Figure 4 suggests a similar concave response, where much of the permanent inundation occurs within the first meter, leaving less additional territory to be lost with subsequent increases (which probably already involve the almost complete flooding of the interior wetland). This highlights the vulnerability of coastal wetlands such as La Albufera, whose current equilibrium depends on a narrow separation from the sea, and even a small rise in sea level can upset this balance and turn large areas of land into permanently flooded expanses.

Similarly, other coastal regions that are smaller in size but low in altitude reflect the same phenomenon. The Cabanes area, for example, has a much smaller flood zone than the Ebro Delta, yet the first SLR meter causes the greatest percentage impact (flooding) in the territory. Although in absolute terms the affected area is smaller, in relative terms the initial +1 m covers the most significant portion of vulnerable land, with subsequent more modest increases in flooded areas with higher SLR. This behavior is consistent with the idea that in flat areas, much of the land is just above the current sea level, so a small rise quickly turns it into intertidal or subtidal areas [36]. On the other hand, once these large low-lying areas are flooded, the land remaining at slightly higher elevations occupies less surface area (often the higher "shores" or land that begins to rise), so that each additional meter covers fewer new flooded areas.

In contrast, there are areas where the relationship is not concave but convex, indicating the presence of some topographical or structural threshold that limits the impact of the first meter but gives way to higher rises. The Tordera Delta is a case in point: there, the first meter is not as damaging as the next two. This suggests that at +1 m, many parts of that area are not yet significantly flooded, but once a certain critical level (between 1 and +2 m) is exceeded, water penetrates inland, flooding large areas at once. In cases like this, with +1 m only ~15% of the area is flooded, but with +2 m this increases to ~52% and with +3 m to over 95% (convex response pattern). This stepped behavior would indicate that current natural or artificial defenses may be effective against modest increases in mean sea level but would not prevent severe flooding in higher elevation scenarios. This flooding pattern is indicative of coastal areas that initially resist, but eventually the water overcomes them when the level rises high enough.

Finally, the case studies with more linear behavior (Delta del Llobregat, Tarragona, Castellón, and Sagunto) correspond to areas where the topography has a fairly uniform slope inland, so that each increase in level covers a similar strip of land. In these cases, there is neither a disproportionate effect of the first meter nor a marked threshold thereafter; simply an approximately constant increase in the flooded area for each meter of SLR is observed. This pattern is common on slightly higher coasts or coastal plains of limited width, where the distribution of heights is approximately homogeneous. For example, an open beach with a low backwash and a constant slope could experience a loss of beach/land area that is almost proportional to the rise in sea level (which, in the absence

of abrupt barriers inland, show very linear relationships between SLR and flooded area in other sections). This means that for these areas, the impact of the second and third meters is as significant as that of the first in terms of new flooded area, with a regular-sustained progression.

In summary, the impact of the first meter of SLR varies by region. In relative terms, ultra-low-lying coastal areas (deltas, coastal lagoons) suffer most of the potential flooding already at +1 m (first "worst" or most critical meter). In contrast, in areas with dunes or urban/protective structures, the first meter may cause relatively little additional damage until the threshold is exceeded (first meter is "benign" compared to the following ones). On the scale of the entire coastline studied, the behavior is more convex because the Albufera and the Ebro Delta represent by far the largest part of the affected territory, compared to the rest, and show this convex (slowed) behavior, so that overall, the first meter of SLR represents a significant percentage of the total area lost. In fact, according to [37], globally, many of the exposed coastal areas and populations are concentrated at very low elevations; for example, in some Caribbean Island countries, more than 70% of the low-lying coastal population lives below +1 m, which means that the first meter of SLR would put the majority at risk. In this study, this phenomenon is manifested territorially: Figure 5 shows the contribution of each sub-region to the total loss of territory under different scenarios, showing that the Ebro Delta contributes the largest part of the flooded area in all scenarios (due to its large size and low elevation), followed in importance by other areas such as the Albufera de Valencia.

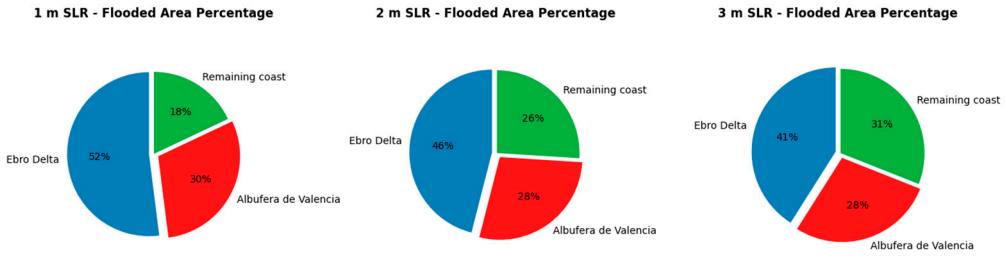


Figure 5. Proportional contribution of each sub-region to the total flooded area under different SLR scenarios (+1 m, +2 m, and +3 m). The pie chart highlights the dominance of ultra-low-lying areas, specifically the Ebro Delta and Albufera de Valencia, in overall territorial loss. These regions account for the largest share of flooded land due to their extensive low-elevation zones, emphasizing the critical impact of the first meter of SLR. The visualization underscores the spatial concentration of vulnerability along the Mediterranean coast.

Across all sea-level rise scenarios (+1 m, +2 m, and +3 m), the Ebro Delta consistently accounts for the largest share of flooded land, followed by the Albufera. These ultra-low-lying systems dominate the overall territorial flood risk, with the Ebro Delta alone representing nearly half of the total inundated area under the +1 m scenario, and still maintaining the highest individual contribution under +3 m. This pattern underscores the disproportionate vulnerability of wide, low-lying deltas, which are repeatedly highlighted in Figure 5, where the Ebro Delta emerges as the most affected region across all evaluated scenarios.

3.5.2. GCFI Calculation

The GCFI results allow coastal sections with different degrees of vulnerability (very low, low, moderate, high, very high) to be identified. By quantifying the total study area (Figure 3), most of the coastline assessed is moderately to highly vulnerable. In general, low-lying and sedimentary coastal areas (deltas, marshes, coastal lagoons) have high or very high GCFI values. For example, the Ebro Delta stands out with a high GCFI in the

global classification of the coast (it is one of the most vulnerable areas of the Catalan coast) due to its flat topography and low altitude. Other flat coastal areas, such as the coastal lagoon of the Albufera de Valencia or the Llobregat delta, also have high GCFI scores, confirming their high physical susceptibility. This characterization using GCFI provides a basis for understanding where the potential impact of SLR would be greatest from a physical standpoint [38].

4. Discussion

This study presents a robust and accessible methodology for estimating flooded areas and deriving CVIs based on publicly available satellite data and pixel-level analysis. The findings from the selected Mediterranean study sites demonstrate both spatial variability in flood exposure and methodological sensitivity to resolution and image tolerance. These observations invite several interpretative considerations regarding the utility, applicability, and limitations of the proposed approach.

One of the key insights derived from the analysis is the non-linear response of coastal systems to SLR. In particular, the results consistently show that the first meter of SLR produces the most substantial changes in flooded areas across all case studies, as illustrated in Figure 4, particularly for the Ebro Delta, Albufera de Valencia, and Cabanes. This behavior reinforces the conclusion that early adaptation efforts should prioritize thresholds below +1 m SLR, since later increments exhibit more moderate additional impacts. These findings are consistent with previous research emphasizing the disproportionate impact of initial inundation in low-lying areas (e.g., [2,39,40]).

Furthermore, although the analysis was based on a static flood model, without accounting for dynamic processes such as wave run-up, storm surge, or evolving coastal defenses, the methodology yields a robust first-order approximation of potential long-term impacts. Similar "bathtub" models have been widely used in regional-scale assessments with limited hydrodynamic data availability [41,42], serving as practical baselines for prioritizing adaptation strategies. The observed non-linear increase in inundated surface, particularly between the +1 m and +2 m SLR scenarios, underscores the relevance of threshold dynamics in exposure escalation and supports the necessity of location-specific vulnerability analyses.

The sensitivity analysis demonstrates that higher-resolution imagery captures more detailed inundation patterns, enabling improved delineation of coastal features and more precise quantification of flooded areas. Unlike dynamic modeling approaches, which often require high-performance computing and complex calibration, the strength of the proposed method lies in its computational simplicity and operational efficiency. Even when applied at higher resolutions, the methodology remains lightweight: the only added requirement is the acquisition of a greater number of input images. The image processing, which is based on binary comparison and pixel subtraction, can be executed on standard personal computers using widely accessible tools such as MATLAB R2021. As such, the proposed method offers an effective balance between accuracy and practicality, making it suitable for both large-scale assessments and applications in resource-limited contexts.

Although the pixel tolerance parameter had a minor effect on the outcomes, the testing performed confirms the robustness of the classification logic. This suggests that image resolution, rather than classification noise, remains the main contributor to uncertainty. Still, pixel tolerance assessments are a useful complementary procedure in confirming internal consistency and should be considered in analogous studies employing raster-based flood classification techniques. In terms of index robustness, the $\pm$5-pixel tolerance produced a negligible effect on whole-domain totals (<0.05% across scenarios, see Table 3), so the a-component seldom shifts classes unless very near a bin threshold. By contrast,

resolution differences up to ~5–6% at coarser scales represent the main driver of potential class changes in edge cases, primarily affecting l and, locally, w; reporting [GCFI^{-}, GCFI^{+}] makes these situations explicit.

The shape, orientation, and depth of flooded areas also emerge as decisive elements in characterizing coastal vulnerability. This behavior reinforces the importance of assessing not only the flooded area but also the geometric properties of the inundation zone, which can influence emergency accessibility, exposure gradients, and potential erosional dynamics. The proposed GCFI offers an enhanced diagnostic lens to interpret not just magnitude but also the spatial footprint of permanent flooding, adding value to conventional CVI approaches by enabling a more nuanced ranking of vulnerability under different SLR scenarios (e.g., [33,43]). While geometric descriptors of flooding (e.g., inland penetration) may qualitatively align with higher susceptibility to shoreline retreat in low-slope sedimentary coasts, these results pertain to permanent inundation, not to erosive shoreline displacement. Establishing a quantitative link would require morphodynamic modeling (waves, sediment transport, profile response) that lies beyond the present scope. For future research, it is possible to benchmark the GCFI against established multi-parameter indices under a harmonized, site-specific dataset to quantify complementarities and limits.

The case of the Albufera de Valencia illustrates the compounding risks faced by low-lying agricultural wetlands. While a +1 m SLR under static conditions might not fully overtop the coastal barrier, the combination of this scenario with episodic storm surges could trigger catastrophic flooding. This emphasizes the need to account for compound hazards, particularly in rice-producing regions where saline intrusion and infrastructure vulnerability intersect under future climate conditions.

Furthermore, the socioeconomic implications of the spatial patterns observed merit attention. As detailed in Section 2.5, a significant proportion of the inundated surface corresponds to tourist beaches or urbanized coastal strips with economic value tied to recreational use and infrastructure. Although not directly modeled in this study, the loss of beach width, erosion of foredunes, and saltwater intrusion into wetlands suggest potential economic losses for tourism, fisheries, and conservation initiatives. These insights support integrating the proposed methodology with land use data and economic impact modeling in future research. Given the concentration of exposure in ultra-low-lying deltas and lagoons and the disproportionate effect of the first +1 m of SLR, we recommend a tiered pathway for decision-making. First, enact zoning and setback policies for lands below the +1 m envelope and along coastal corridors identified as high/very-high by the GCFI (screening). Secondly, priority should be given to nature-based solutions, such as the restoration of dune [44] and foredunes [45], the conservation of wetland areas [46], the combination of these with hybrid solutions [47] and targeted hardening of critical infrastructure, complemented (where data permit) by dynamic modeling that accounts for defenses and compound flooding (appraisal). Third, consider managed realignment or relocation only where detailed studies project recurrent loss of access or unacceptable risk and where protection proves disproportionate in cost or environmental impact (implementation). This screening-to-appraisal sequence avoids blanket relocation recommendations based solely on static mapping while providing actionable, low-regret steps for at-risk areas.

Because static inundation surfaces ignore defense performance and operational measures, the resulting extents represent an upper-bound envelope consistent with a no-defense or defense-failure condition. This framing is useful for contingency planning and risk communication, helping to identify locations where failure would be unacceptable and therefore warrant targeted protection/maintenance or, alternatively, managed realignment in subsequent, site-specific appraisals.

Lastly, the limitations of the static bathtub model must be acknowledged. Effective coastal water levels vary spatially due to wave set-up, storm surge, tidal modulation, groundwater interactions, and the partial performance of dunes, levees, and engineered defenses. Accordingly, the static surfaces used here should be interpreted as mean water-level exceedance envelopes rather than fully dynamic flood extents. The results are framed as a first-order exposure screening to be complemented, where data permit, with dynamic modeling and explicit evaluation of defense performance. The approach does not resolve dynamic flood attenuation or friction, tidal amplification, the partial performance of natural or engineered defenses under load, groundwater-table interactions, or the operation/failure of pumping infrastructure. These processes require site-specific, process-based modeling beyond the scope of the present screening. In addition, vertical uncertainties in the source elevation product—particularly in flat, vegetated coastal lowlands—may affect absolute inundation footprints and should be addressed in site-specific studies with ground-validated, bare-earth DTMs or GNSS control. Likewise, the use of a uniform SRTM-derived source emphasizes cross-site comparability over local vertical precision. Higher-resolution, locally calibrated DTMs are recommended for site-specific appraisals and design studies. Because outputs are reported in image coordinates calibrated to meters-per-pixel, they are suitable for screening and inter-scenario comparisons, but not for direct overlay with external GIS baselines. These constraints imply that the approach may overestimate flooding in some areas and underestimate it in others. Nonetheless, its simplicity and replicability make it a valuable first-order screening tool for preliminary SLR impact assessment, especially when combined with participatory planning or scenario development for climate adaptation.

While this study focused on physical exposure derived from topography-based inundation mapping, future extensions of the methodology could incorporate demographic and economic datasets to provide a more integrated assessment of flood risk. For example, overlaying land use information, infrastructure data, or population density layers (e.g., from census records or OpenStreetMap) onto the flooded zones would enable the identification of critical assets and vulnerable groups, which is essential for risk-informed planning and targeted adaptation measures.

5. Conclusions

This study introduces a reproducible and scalable methodology to assess coastal flood exposure under sea-level rise scenarios by leveraging SRTM-based inundation imagery and pixel-level comparison techniques. The approach relies on publicly accessible satellite data and basic image subtraction techniques, ensuring its replicability and utility across multiple spatial scales. The method allows the quantification of flooded areas under incremental SLR scenarios and provides a foundation for the calculation of a composite CVI enhanced by the introduction of a GCFI to evaluate vulnerability across diverse coastal settings.

Key conclusions include:

Reproducible and scalable methodology: This study introduces a pixel-based approach using satellite imagery to assess coastal flood exposure under sea-level rise (SLR) scenarios, requiring minimal computational resources;

Vulnerability patterns: The GCFI captures the shape and inland penetration of flood footprints, enabling comparative vulnerability screening that complements area-based metrics and conventional CVIs. Deltas and coastal lagoons emerge as the most critical areas due to their low elevation and rapid inundation, highlighting the need for early adaptation strategies;

Methodological factors and applicability: Image resolution and tolerance significantly influence inundation estimates, emphasizing the importance of methodological consistency.

The proposed GCFI provides a cost-effective tool for preliminary vulnerability assessments in data-scarce regions;

Planning potential and future improvements: The method supports preliminary coastal-risk screening, land-use zoning, and prioritization of adaptation and can be complemented with dynamic flood models, land-use data, and socioeconomic layers where available to enhance operational relevance. This methodology supports preliminary coastal-risk screening, land-use zoning, and prioritization of adaptation. A tiered pathway is recommended rather than generalized relocation based solely on static screening: (i) setbacks below the +1 m envelope in high/very-high GCFI corridors; (ii) nature-based/hybrid protection with site-specific dynamic appraisal; and (iii) managed realignment only where detailed studies indicate recurrent, unacceptable risk.

In summary, this study presents an innovative and operationally efficient methodology that integrates static flood mapping, resolution-sensitivity analysis, and the GCFI within a unified, computationally lightweight framework. Despite inherent limitations (most notably, the exclusion of dynamic forcing mechanisms), its methodological simplicity and adaptability render it a valuable tool for coastal vulnerability assessment. The application of the GCFI facilitates the classification of coastal segments based on relative vulnerability, with areas of very high susceptibility typically corresponding to low-lying, geomorphologically flat environments such as deltas and coastal lagoons, whereas urbanized coastal zones generally exhibit lower vulnerability. This pixel-based approach enhances traditional assessment techniques that often rely on high-resolution DEMs and high-performance computing resources, offering a scalable and accurate alternative particularly suited for large-scale screening in data-scarce or resource-constrained contexts. Furthermore, the framework provides a robust basis for comparative analysis with SLR inundation scenarios, enabling verification of spatial risk manifestation and supporting the prioritization of adaptation strategies in the most exposed regions. For site-specific applications and design studies, the use of ground-validated, bare-earth elevation data (e.g., LiDAR DTMs and GNSS control) is recommended to refine absolute flood extents and reduce vertical-bias uncertainty. For transparency, per-site GCFI bounds [$GCFI^{-}$; $GCFI^{+}$] are reported based on the propagation of resolution and boundary-tolerance perturbations. In most cases, the resulting vulnerability class remains unchanged, thereby explicitly indicating class stability in edge cases.

Author Contributions: Conceptualization, C.M., M.V., A.S.-A. and V.G.; methodology, C.M., A.S.-A. and D.G.; software, M.V., C.A. and C.M.; validation, C.M., V.G., M.V., F.C.-V. and D.G.; formal analysis, C.M., J.P.S. and A.S.-A.; investigation, C.M. and M.V.; resources, D.G. and A.S.-A.; data curation, C.M., M.V. and C.A.; writing—original draft preparation, C.M., M.V., F.C.-V. and J.P.S.; writing—review and editing, C.M., A.S.-A. and J.P.S.; visualization, M.V. and V.G.; supervision, A.S.-A.; project administration, D.G. and A.S.-A.; funding acquisition, A.S.-A. All authors have read and agreed to the published version of the manuscript.

Funding: This project has received funding from the European Union's Horizon 2020 research and innovation programme under grant agreement No 101037097 (REST-COAST project).

Data Availability Statement: Images are available at flood.firetree.net platform and codes will be available upon request.

Acknowledgments: The authors gratefully acknowledge the support of two major funded initiatives. First, the REST-COAST project ("Large-scale RESToration of COASTal ecosystems through rivers-to-sea connectivity"), coordinated by the Universitat Politècnica de Catalunya which contributed with methodologies based on nature-based solutions, restorational simulations, and observational data for science-informed decision-making. Second, sincere thanks are extended to the BARRACLIM project ("Barraques Climàtiques per adaptar la costa i les seves activitats a condicions futures"), funded by

the Generalitat de Catalunya, Departament d'Acció Climàtica, Alimentació i Agenda Rural (Reference No ACC_2023_EXP_SIA002_09_0001569). The authors also thank all REST-COAST and BARRACLIM partners and team members for their collaboration, insightful discussions, and data sharing, which were essential for developing and refining the methodological approach presented here.

Conflicts of Interest: The authors declare no conflicts of interest.

Abbreviations

The following abbreviations are used in this manuscript:

SLR	Sea Level Rise
DEM	Digital Elevation Model
GCFI	Geomorphic Coastal Flooding Index
CVI	Coastal Vulnerability Indices
IPCC	Intergovernmental Panel on Climate Change
RCP	Representative Concentration Pathways
NASA's SRTM	National Aeronautics and Space Administration's Shuttle Radar Topography Mission
BMP	BitMaP
LiDAR	Light Detection And Ranging

References

1. López-Dóriga, U.; Jiménez, J.A. Impact of Relative Sea-Level Rise on Low-Lying Coastal Areas of Catalonia, NW Mediterranean, Spain. *Water* **2020**, *12*, 3252. [CrossRef]
2. Lomelí-Quintero, V.-M.; Calderón-Vega, F.; Mösso, C.; Sánchez-Arcilla, A.; García-Soto, A.-D. Impact Costs Due to Climate Change along the Coasts of Catalonia. *J. Mar. Sci. Eng.* **2023**, *11*, 1939. [CrossRef]
3. Mösso, C.; Gracia, V.; Mestres, M.; Sierra, J.P.; Sánchez-Arcilla, A. Sediment Mobility at Fangar Bay Entrance (NW Spanish Mediterranean): Management Implications Under Present and Future Climates. *J. Coast. Res.* **2020**, *95*, 894–899. [CrossRef]
4. Sánchez-Arcilla, A.; González-Marco, D.; Bolãnos, R. A review of wave climate and prediction along the Spanish Medi-terranean coast. *Nat. Hazards Earth Syst. Sci.* **2008**, *8*, 1217–1228. [CrossRef]
5. Sierra, J.P.; Casanovas, I.; Mösso, C.; Mestres, M.; Sánchez-Arcilla, A. Vulnerability of Catalan (NW Mediterranean) ports to wave overtopping due to different scenarios of sea level rise. *Reg. Environ. Change* **2016**, *16*, 1457–1468. [CrossRef]
6. Oppenheimer, M.; Glavovic, B.C.; Hinkel, J.; van de Wal, R.; Magnan, A.K.; Abd-Elgawad, A.; Cai, R.; Cifuentes-Jara, M.; DeConto, R.M.; Ghosh, T.; et al. Sea Level Rise and Implications for Low-Lying Islands, Coasts and Communities. In *IPCC Special Report on the Ocean and Cryosphere in a Changing Climate*; Pörtner, H.-O., Roberts, D.C., Masson-Delmotte, V., Zhai, P., Tignor, M., Poloczanska, E., Mintenbeck, K., Alegría, A., Nicolai, M., Okem, A., Eds.; Intergovernmental Panel on Climate Change (IPCC): Geneva, Switzerland, 2019.
7. Vacchi, M.; Joyse, K.M.; Kopp, R.E.; Marriner, N.; Kaniewski, D.; Rovere, A. Climate pacing of millennial sea-level change variability in the central and western Mediterranean. *Nat. Commun.* **2021**, *12*, 4013. [CrossRef]
8. Sánchez-Arcilla, A.; Gracia, V. Coastal Adaptation Pathways and Tipping Points for Typical Mediterranean Beaches under Future Scenarios. *J. Mar. Sci. Eng.* **2024**, *12*, 1063. [CrossRef]
9. Higgins, S.A. Review: Advances in delta-subsidence research using satellite methods. *Hydrogeol. J.* **2016**, *24*, 587–600. [CrossRef]
10. Tay, C.; Lindsey, E.O.; Chin, S.T.; McCaughey, J.W.; Bekaert, D.; Nguyen, M.; Hua, H.; Manipon, G.; Karim, M.; Horton, B.P.; et al. Sea-level rise from land subsidence in major coastal cities. *Nat. Sustain.* **2022**, *5*, 1049–1057. [CrossRef]
11. Vermaat, J.E.; Eleveld, M.A. Divergent options to cope with vulnerability in subsiding deltas. *Clim. Change* **2013**, *117*, 31–39. [CrossRef]
12. Sánchez-Artús, X.; Gracia, V.; Espino, M.; Grifoll, M.; Simarro, G.; Guillén, J.; González, M.; Sanchez-Arcilla, A. Operational hydrodynamic service as a tool for coastal flood assessment. *Ocean Sci.* **2025**, *21*, 749–766. [CrossRef]
13. Viñes, M.; Sánchez-Arcilla, A.; Epelde, I.; Mösso, C.; Franco, J.; Sospedra, J.; Abalia, A.; Líria, P.; Grifoll, M.; Ojanguren, A.; et al. Morphodynamic predictions based on Machine Learning. Performance and limits for pocket beaches near the Bilbao port. *Front. Environ. Sci.* **2025**, *13*, 1600473. [CrossRef]
14. Pereira, R.L.M.C.; Mösso, C.; Pereira, L.C.C. Assessment of Vulnerability to Erosion in Amazonian Beaches. *Geographies* **2025**, *5*, 29. [CrossRef]
15. Pendleton, E.A.; Theiler, E.R.; Williams, S.J. *Coastal Vulnerability Assessment of Cape Hatteras National Seashore (CAHA) to Sea-Level Rise*; U.S. Geological Survey: Reston, VA, USA, 2005. [CrossRef]

16. Gornitz, V.M.; White, T.W.; Daniels, R.C. A Coastal Hazards Data Base for the US East Coast. Tennessee, United States, Aug. 1992. Available online: https://digital.library.unt.edu/ark:/67531/metadc1182892/ (accessed on 27 August 2025).
17. Díaz-Delgado, R.; Aragonés, D.; Afán, I.; Bustamante, J. Long-Term Monitoring of the Flooding Regime and Hydroperiod of Doñana Marshes with Landsat Time Series (1974–2014). *Remote Sens.* **2016**, *8*, 775. [CrossRef]
18. Cavallo, C.; Papa, M.N.; Gargiulo, M.; Palau-Salvador, G.; Vezza, P.; Ruello, G. Continuous Monitoring of the Flooding Dynamics in the Albufera Wetland (Spain) by Landsat-8 and Sentinel-2 Datasets. *Remote Sens.* **2021**, *13*, 3525. [CrossRef]
19. Soria, J.M.; Muñoz, R.; Campillo-Tamarit, N.; Molner, J.V. Flash-Flood-Induced Changes in the Hydrochemistry of the Albufera of Valencia Coastal Lagoon. *Diversity* **2025**, *17*, 119. [CrossRef]
20. Nicholls, R.J.; Cazenave, A. Sea-Level Rise and Its Impact on Coastal Zones. *Science* **2010**, *328*, 1517–1520. [CrossRef]
21. Vitousek, S.; Barnard, P.L.; Fletcher, C.H.; Frazer, N.; Erikson, L.; Storlazzi, C.D. Doubling of coastal flooding frequency within decades due to sea-level rise. *Sci. Rep.* **2017**, *7*, 1399. [CrossRef]
22. Hinkel, J.; Lincke, D.; Vafeidis, A.T.; Perrette, M.; Nicholls, R.J.; Tol, R.S.J.; Marzeion, B.; Fettweis, X.; Ionescu, C.; Levermann, A. Coastal flood damage and adaptation costs under 21st century sea-level rise. *Proc. Natl. Acad. Sci. USA* **2014**, *111*, 3292–3297. [CrossRef]
23. Vousdoukas, M.I.; Mentaschi, L.; Voukouvalas, E.; Verlaan, M.; Jevrejeva, S.; Jackson, L.P.; Feyen, L. Global probabilistic projections of extreme sea levels show intensification of coastal flood hazard. *Nat. Commun.* **2018**, *9*, 2360. [CrossRef] [PubMed]
24. Vafeidis, A.T.; Schuerch, M.; Wolff, C.; Spencer, T.; Merkens, J.L.; Hinkel, J.; Lincke, D.; Brown, S.; Nicholls, R.J. Water-level attenuation in global-scale assessments of exposure to coastal flooding: A sensitivity analysis. *Nat. Hazards Earth Syst. Sci.* **2019**, *19*, 973–984. [CrossRef]
25. Kulp, S.; Strauss, B.H. Global DEM Errors Underpredict Coastal Vulnerability to Sea Level Rise and Flooding. *Front. Earth Sci.* **2016**, *4*, 36. [CrossRef]
26. Fewtrell, T.J.; Bates, P.D.; Horritt, M.; Hunter, N.M. Evaluating the effect of scale in flood inundation modelling in urban environments. *Hydrol. Process.* **2008**, *22*, 5107–5118. [CrossRef]
27. Savage, J.T.S.; Bates, P.; Freer, J.; Neal, J.; Aronica, G. When does spatial resolution become spurious in probabilistic flood inundation predictions? *Hydrol. Process.* **2016**, *30*, 2014–2032. [CrossRef]
28. Ozdemir, H.; Sampson, C.C.; de Almeida, G.A.M.; Bates, P.D. Evaluating scale and roughness effects in urban flood modelling using terrestrial LIDAR data. *Hydrol. Earth Syst. Sci.* **2013**, *17*, 4015–4030. [CrossRef]
29. Sanders, B.F. Evaluation of on-line DEMs for flood inundation modeling. *Adv. Water Resour.* **2007**, *30*, 1831–1843. [CrossRef]
30. Wing, O.E.J.; Bates, P.D.; Smith, A.M.; Sampson, C.C.; Johnson, K.A.; Fargione, J.; Morefield, P. Estimates of present and future flood risk in the conterminous United States. *Environ. Res. Lett.* **2018**, *13*, 034023. [CrossRef]
31. Li, J.; Wong, D.W. Effects of DEM sources on hydrologic applications. *Comput. Environ. Urban Syst.* **2010**, *34*, 251–261. [CrossRef]
32. Sampson, C.C.; Smith, A.M.; Bates, P.D.; Neal, J.C.; Alfieri, L.; Freer, J.E. A high-resolution global flood hazard model. *Water Resour. Res.* **2015**, *51*, 7358–7381. [CrossRef]
33. Thieler, E.R.; Hammar-Klose, E.S. *National Assessment of Coastal Vulnerability to Sea-Level Rise: Preliminary Results for the U.S. Pacific Coast*; U.S. Geological Survey: Reston, VA, USA, 2000. [CrossRef]
34. Torresan, S.; Critto, A.; Rizzi, J.; Marcomini, A. Assessment of coastal vulnerability to climate change hazards at the regional scale: The case study of the North Adriatic Sea. *Nat. Hazards Earth Syst. Sci.* **2012**, *12*, 2347–2368. [CrossRef]
35. Mclaughlin, S.; Cooper, J.A.G. A multi-scale coastal vulnerability index: A tool for coastal managers? *Environ. Hazards* **2010**, *9*, 233–248. [CrossRef]
36. Alvarado-Aguilar, D.; Jiménez, J.A.; Nicholls, R.J. Flood hazard and damage assessment in the Ebro Delta (NW Mediterranean) to relative sea level rise. *Nat. Hazards* **2012**, *62*, 1301–1321. [CrossRef]
37. Nicholls, R.; Hanson, S.; Herweijer, C.; Ranger, N.; Hallegatte, S.; Corfee-Morlot, J.; Chateau, J.; Muir-Wood, R. Ranking Port Cities with High Exposure and Vulnerability to Climate Extremes: Exposure Estimates. In *OECD Environment Working Papers, No. 1.*; OECD Publishing: Paris, France, 2008. [CrossRef]
38. Losada, J.I.; Méndez, J.F.; Olabarrieta, M.; Liste, M.; Menéndez, M.; Abascal, A.J.; Tomás, A.; Agudelo, R.; Guanche, R.; Santamaría-Medina, R. Impactos en La Costa Española por Efecto del Cambio Climático, Santander. 2002. Available online: https://www.miteco.gob.es/content/dam/miteco/es/cambio-climatico/temas/impactos-vulnerabilidad-y-adaptacion/fase3_costas_tcm30-178538.pdf#:~:text=El%20%C3%ADndice%20de%20vulnerabilidad%20costera,III.%203.11 (accessed on 21 July 2025).
39. Nicholls, R.J.; Wong, P.P.; Burkett, V.R.; Codignotto, J.O.; Hay, J.E.; Mclean, R.F.; Ragoonaden, S.; Woodroffe, C.D.; Abuodha, P.; Arblaster, J.; et al. Coastal systems and low-lying areas. In *Climate Change 2007: Impacts, Adaptation and Vulnerability. Contribution of Working Group II to the Fourth Assessment Report of the Intergovernmental Panel on Climate Change*; Cambridge University Press: Cambridge, UK, 2007; pp. 315–356.
40. Vousdoukas, M.I.; Ranasinghe, R.; Mentaschi, L.; Plomaritis, T.A.; Athanasiou, P.; Luijendijk, A.; Feyen, L. Sandy coastlines under threat of erosion. *Nat. Clim. Change* **2020**, *10*, 260–263. [CrossRef]

41. Schuerch, M.; Spencer, T.; Temmerman, S.; Kirwan, M.L.; Wolff, C.; Lincke, D.; McOwen, C.J.; Pickering, M.D.; Reef, R.; Vafeidis, A.T.; et al. Future response of global coastal wetlands to sea-level rise. *Nature* **2018**, *561*, 231–234. [CrossRef] [PubMed]
42. Lichter, M.; Vafeidis, A.T.; Nicholls, R.J. Exploring Data-Related Uncertainties in Analyses of Land Area and Population in the "Low-Elevation Coastal Zone" (LECZ). *J. Coast. Res.* **2010**, *27*, 757. [CrossRef]
43. Ramieri, E.; Hartley, A.; Barbanti, A.; Santos, F.; Gomes, A.; Hildén, M.; Laihonen, P.; Marinova, N.; Santini, M. *Methods for Assessing Coastal Vulnerability to Climate Change*; ETC CCA Technical Paper 1/2011; European Environment Agency: Copenhagen, Denmark, 2011. [CrossRef]
44. Johnston, K.K.; Dugan, J.E.; Hubbard, D.M.; Emery, K.A.; Grubbs, M.W. Using dune restoration on an urban beach as a coastal resilience approach. *Front. Mar. Sci.* **2023**, *10*, 1187488. [CrossRef]
45. Sigren, J.M.; Figlus, J.; Armitage, A.R. Coastal Sand Dunes and Dune Vegetation: Restoration, Erosion, and Storm Protection. 2014. Available online: https://api.semanticscholar.org/CorpusID:134823563 (accessed on 27 August 2025).
46. Van Coppenolle, R.; Temmerman, S. Identifying global hotspots where coastal wetland conservation can contribute to nature-based mitigation of coastal flood risks. *Glob. Planet. Change* **2020**, *187*, 103125. [CrossRef]
47. Waryszak, P.; Gavoille, A.; Whitt, A.A.; Kelvin, J.; Macreadie, P.I. Combining gray and green infrastructure to improve coastal resilience: Lessons learnt from hybrid flood defenses. *Coast. Eng. J.* **2021**, *63*, 335–350. [CrossRef]

Disclaimer/Publisher's Note: The statements, opinions and data contained in all publications are solely those of the individual author(s) and contributor(s) and not of MDPI and/or the editor(s). MDPI and/or the editor(s) disclaim responsibility for any injury to people or property resulting from any ideas, methods, instructions or products referred to in the content.